The application of scanning Doppler wind lidars and retrieved meteorological fields in a 3-D space to study boundary layer characteristics

廖宇慶 [1*], 楊伯謙 [1], 陳韡鼐 [2], 李育棋 [3], 許玉金 [3]

蔡嘉倫 [4], 林沛練 [1], 蘇柏林 [5], 藍嘉偉 [6], 蔡世樵 [7]

[1*]國立中央大學大氣科學系
[2] 中央研究院環境變遷研究中心
[3] 交通部中央氣象署
[4] 中國文化大學大氣科學系
[5] 慧技科學有限公司
[6] 交通部民用航空局
[7] 國防大學理工學院環境資訊與工程學系

摘要

Through the use of advanced data retrieval techniques and two scanning Doppler wind lidars, the high-resolution (50 m) three-dimensional wind and thermodynamic fields under a clear sky are retrieved and utilized to study the temporal and spatial characteristics of the boundary layer. This work demonstrates the potential advantages of running the proposed approach continuously. Such synthesis methods and high-quality data sets could be applied in the future for various purposes including the study of the boundary layer evolution, initiation of afternoon thunderstorms, air pollutant dispersion, numerical model verification, and real-time monitoring of aviation safety at airports.

關鍵字: 掃描式都卜勒風光達，資料反演，大氣邊界層
Keywords: Scanning Doppler wind LiDAR, Data retrieval, Atmospheric boundary layer

1. Methodology

a. WISSDOM: A multiple-Doppler-lidar/radar 3-D wind synthesis method for use over complex terrain

The WISSDOM algorithm (Liou et al. 2012) used for wind analysis solves for the 3-D wind fields by variationally minimizing a cost function (J_1^{WIS}) expressed by Eq. (1) in which four major equations are implemented:

$$J^{WIS}(u,v,w) = \sum_{M=1}^{4} J_M^{WIS} \tag{1}$$

$$J_1^{WIS} = \sum_{x,y,z}\sum_{i=1}^{N} \alpha_1[(V_r)_i - \frac{(x-P_x^i)}{r_i}u - \frac{(y-P_y^i)}{r_i}v - \frac{(z-P_z^i)}{r_i}w]^2 \tag{2a}$$

$$r_i = \sqrt{(x-P_x^i)^2 + (y-P_y^i)^2 + (z-P_z^i)^2} \tag{2b}$$

$$J_2^{WIS} = \sum_{x,y,z} \alpha_2 \left[\frac{\partial(\rho_0 u)}{\partial x} + \frac{\partial(\rho_0 v)}{\partial y} + \frac{\partial(\rho_0 w)}{\partial z}\right]^2 \tag{3}$$

$$J_3^{WIS} =$$

$$\sum_{x,y,z} \alpha_3 \left[\frac{\partial \xi}{\partial t} + u\frac{\partial \xi}{\partial x} + v\frac{\partial \xi}{\partial y} + w\frac{\partial \xi}{\partial z} + (\xi + f)\left(\frac{\partial u}{\partial x} + \frac{\partial v}{\partial y}\right) + \left(\frac{\partial w}{\partial x}\frac{\partial v}{\partial z} - \frac{\partial w}{\partial y}\frac{\partial u}{\partial z}\right)\right]^2 \tag{4a}$$

$$\xi = \left(\frac{\partial v}{\partial x} - \frac{\partial u}{\partial y}\right) \tag{4b}$$

$$J_4^{WIS} = \sum_{x,y,z} \alpha_4 \left(\vec{V}_H - \vec{V}_{H,B}\right)^2 \tag{5}$$

Eq. (2a) stands for the geometric relationship between the radial velocity $(V_r)_i$ measured by the i^{th} Doppler lidar and the retrieved 3-D Cartesian wind components (u, v, w), where (P_x^i, P_y^i, P_z^i) depicts the coordinates of the ith lidar; r_i is for the distance from each point to the i^{th} lidar; N is the total number of lidars. Eq. (3) is the anelastic continuity equation. Eq. (4a) is the vertical vorticity equation. Eq. (5) represents using a background wind field $(\vec{V}_{H,B})$ to fill in the data-void regions, and provide information for $\vec{V}_H$ in this area. WISSDOM adopts Immersed Boundary Method (IBM) to deal with the terrain.

b. TPTRS: A thermodynamic retrieval scheme over complex terrain

The TPTRS developed by Liou et al. (2019) is utilized to retrieve the thermodynamic variables.

$$\frac{1}{\theta_0}\left[\frac{\partial u}{\partial t} + \vec{V}\cdot\nabla u - fv + turb(u)\right] = -\frac{\partial \pi'}{\partial x} \equiv -F; \tag{6}$$

$$\frac{1}{\theta_0}\left[\frac{\partial v}{\partial t} + \vec{V}\cdot\nabla v + fu + turb(v)\right] = -\frac{\partial \pi'}{\partial y} \equiv -G\,; \tag{7}$$

$$\frac{1}{\theta_0}\left[\frac{\partial w}{\partial t} + \vec{V}\cdot\nabla w + turb(w)\right] = -\frac{\partial \pi'}{\partial z} + g\frac{\theta'}{\theta_0^2} \equiv -H, \tag{8}$$

π' is the perturbation of the normalized pressure, θ' is the potential temperature perturbation from its basic state θ_0. The values of *F*, *G*, and *H* can be obtained once the air motion (*u*, *v*, *w*) is obtained from WISSDOM. In TPTRS the optimal solutions of π' and θ' are obtained variationally which could make Eq. (6)-(8) satisfied in a least square sense.

2. Experiment TZT

a. Experimental design

The dual-lidar field experiment was conducted in Tian-Zhong Township (TZT) near the western coast of Taiwan (Fig. 1a) from 19 to 22 September 2023. The analysis domain showing the locations of various instruments is displayed in Fig. 1b, covering a horizontal area of 6.0 km × 6.0 km.

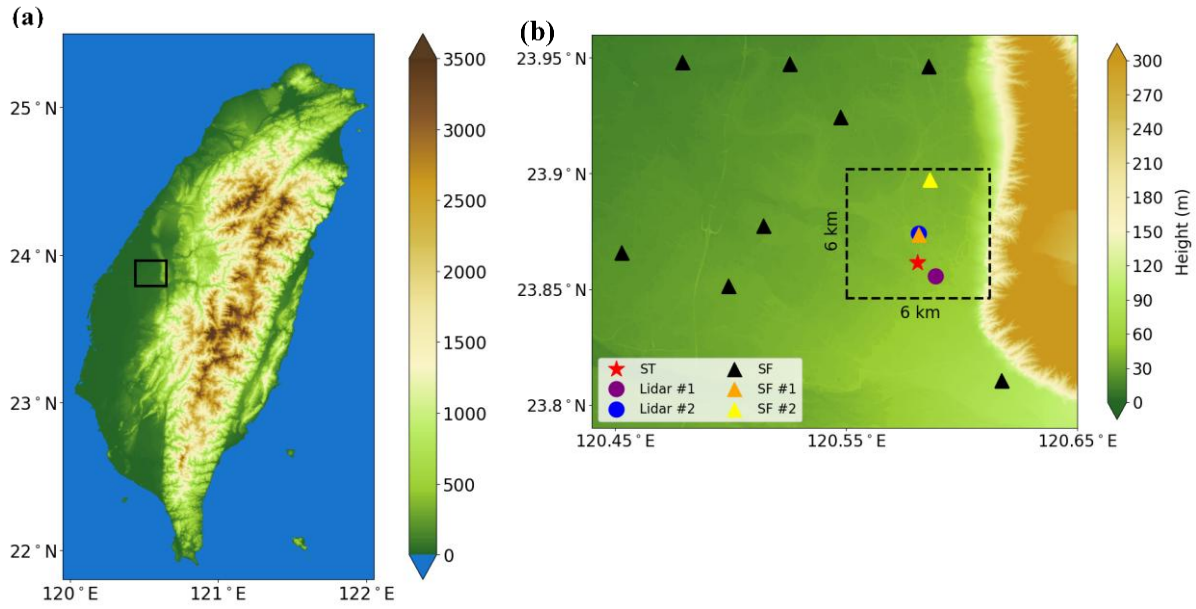

Figure 1 (a) The map of Taiwan island. The location of Tian-Zhong Township is depicted by the black square and enlarged in (b); (b) The area surrounding the analysis domain, which is shown by the square enclosed by dashed lines. The red star is the location of the "Storm Tracker (ST)". The purple and blue circles denote lidar #1 and lidar #2, while the orange and yellow triangles represent surface stations #1 and #2 (SF#1 and SF#2), respectively. The black triangles indicate the surface stations (SF) outside of the analysis domain. The terrain height (m) is depicted by color shading.

b. Results of dual-lidar 3-D wind synthesis

Figure 2 depicts the WISSDOM-retrieved 3-D winds at 1200 LST on 20 September. The prevailing wind is from the ocean toward the west. Updrafts and downdrafts can be found in the central part of the domain. Figures 3 and 4 illustrate an overall comparison between the WISSDOM-retrievals and the

Strom Tracker (ST) observations. Note that ST is a mini-sounding system.

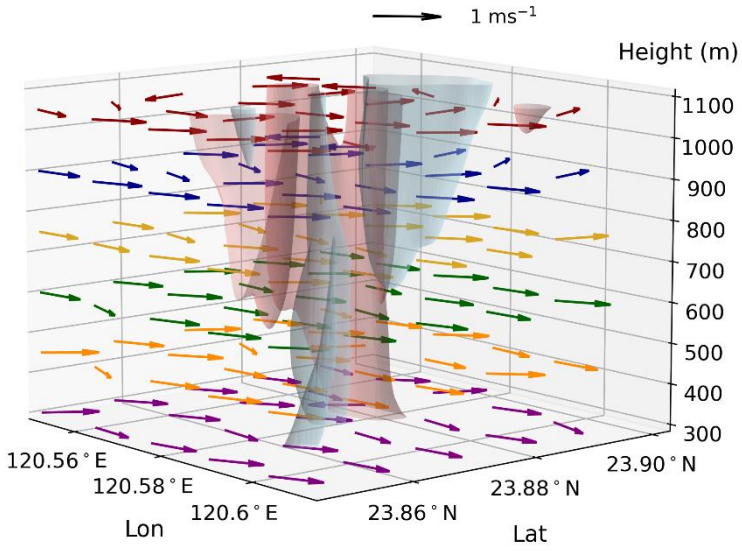

Figure 2 The WISSDOM-retrieved 3-D wind fields at 1200 LST on 20 September. For clarity, the horizontal wind vectors are shown only at 300 m (purple), 450 m (orange), 600 m (green), 750 m (yellow), 900 m (blue), and 1050m (red) in height. Iso-surfaces with a constant vertical wind speed of 1.0 m s^{-1} and -1.0 m s^{-1} are plotted by light coral and light blue, respectively.

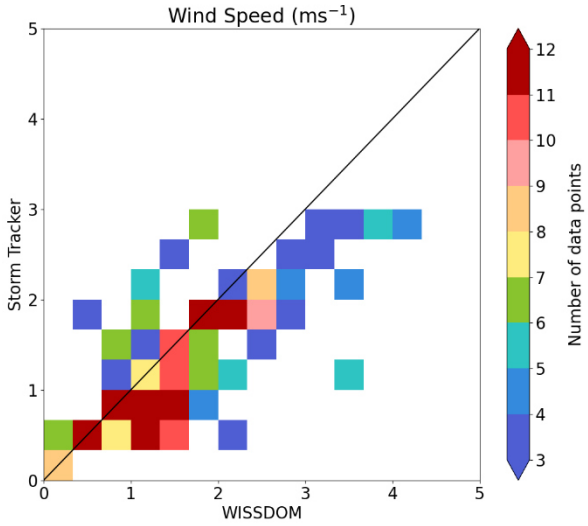

Figure 3 The scatterplot of the WISSDOM-retrieved and ST-observed wind speed (m s^{-1}) for experiment TZT. The color shading denotes the number of data points. The correlation between the retrievals and ST observation is 0.70 for wind speed.

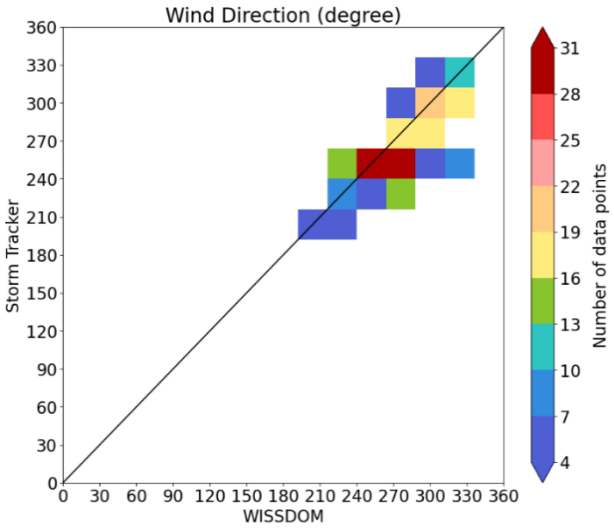

Figure 4 The same as Fig. 3, but for the wind direction (degree). The root-mean-square-differences (RMSDs) for wind speed and wind direction are 0.82 m s^{-1} and 24.7°, respectively.

c. Land-Sea breeze signals on 20 September 2023

Figure 5 shows the time-height display of the wind component perpendicular to the coastline obtained by WISSDOM, ST and surface stations. Westerly/easterly winds stand for sea/land breeze. All three means (WISSDOM, ST, surface station) are able to reveal the land-sea breeze signal, but only the WISSDOM can provide a complete description regarding the structure and evolution of the land-sea breeze.

Figure 5 also reveals that a nocturnal low-level wind maximum can be found at Z=500 m ~ 800 m in the early morning of 20 September. At 1800 LST on 19 September (the sunset time in the previous day), the wind speed and direction are 1.85 m s^{-1} and 200° for horizontal wind, and 1.19 m s^{-1} and 256.6° for geostrophic wind. Thus, the direction of the ageostrophic wind is approximately 157.8°, as shown in Fig. 6. Theoretically, the time needed for the wind speed maximum to occur is when the ageostrophic wind aligns with the geostrophic wind:

$$\frac{12h}{\sin(23.86^o)} \times \frac{(256.6^o - 157.8^o)}{360^o} \sim 8\ hours\ . \quad (9)$$

Thus, the nocturnal low-level wind maximum is expected to occur approximately 8 hours after sunset (1800 LST) on 19 September, or about 0200 LST on 20 September.

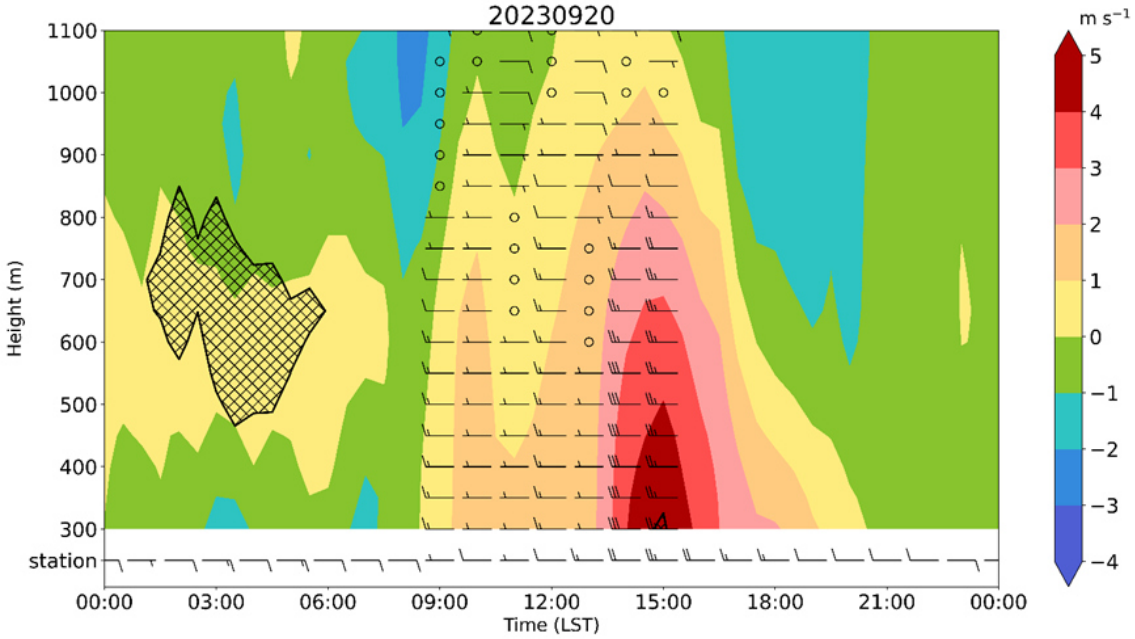

Figure 5 Time-height plot of the wind component perpendicular to the coast line obtained from dual-lidar synthesis (color shading), ST observations (wind barbs from 300 m to 1100 m), and surface station measurements (wind barbs at the bottom) on 20 September 2023. Winds with full barb and half barb represent 1.0 m s^{-1} and 0.5 m s^{-1}, respectively. Positive and negative velocities represent sea breeze and land breeze, respectively. The hatching depicts the area where the total wind speed is greater than 5.0 m s^{-1}. The small circles denote the wind speed detected by ST is less than 0.5 m s^{-1}.

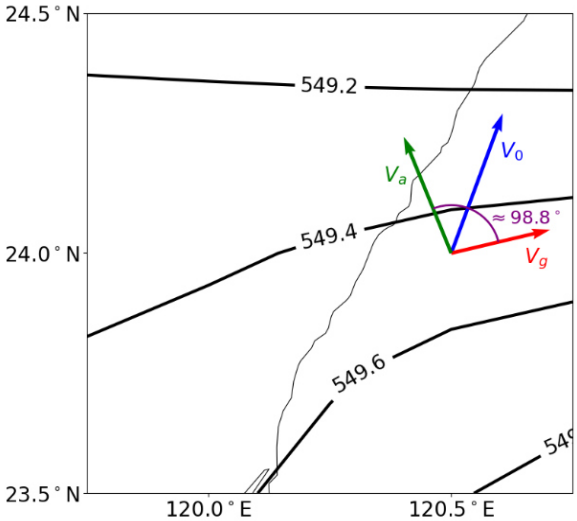

Figure 6 The relationship between the geostrophic wind (V_g, red arrow from ERA5), horizontal wind (V_0, blue arrow from ERA5), and ageostrophic wind (Va, green arrow) at 950 hPa. The wind directions of V_g and V_0 are 256.6° and 200°, respectively. The thick contour lines are geopotential heights (m).

d. Verification of the thermodynamic retrievals and the temporal variation revealed by the retrieved surface pressure and temperature

Figure 7 shows that over 3.5 consecutive days, the retrieved pressure and temperature perturbations are highly consistent with the observations at the surface station. The temperature perturbation reveals a diurnal cycle with a peak value of about 29.5 ºC occurring around 1200 LST, while the pressure perturbation exhibits a semi-diurnal cycle with two minimum values taking place at approximately 1600 LST and 0500 LST.

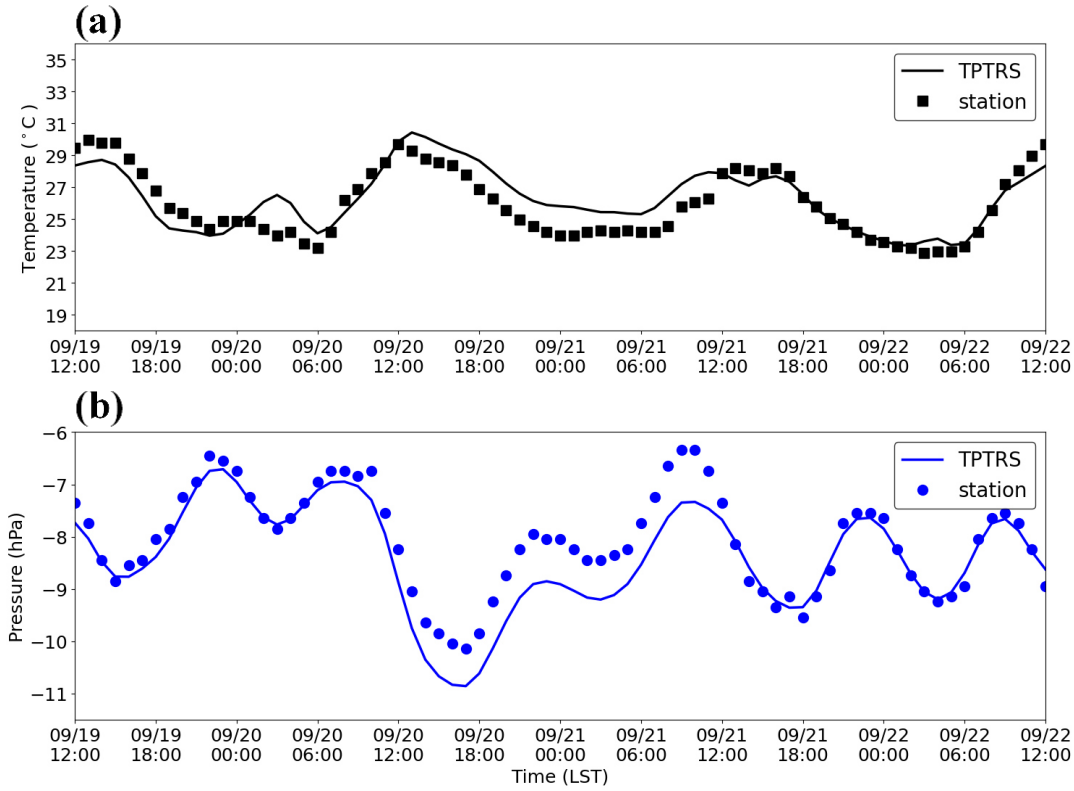

Figure 7 (a) Time series of temperature (ºC) observed by surface station #1 (black square) and retrieved by TPTRS (black line) from 1200 LST 19 September to 1200 LST 22 September 2023. (b) Same as (a), but for the time series of pressure (hPa) observed by surface station #1 (blue circles) and retrieved by TPTRS (blue line).

e. Retrieved 2-D and 3-D thermodynamic fields

Figure 8 depicts the retrieved 3-D potential temperature field at 1200 LST on 20 September. The upright structure of the iso-surface with a potential temperature equal to 308 K suggests that the boundary layer is well-mixed. Figure 9 shows the retrieved two-dimensional temperature field at 1200 LST on 20 September at two different heights (300 m, 900 m), superimposed by the horizontal and vertical velocities. The structures of the kinematic and

thermodynamic fields and their relationships can be clearly revealed.

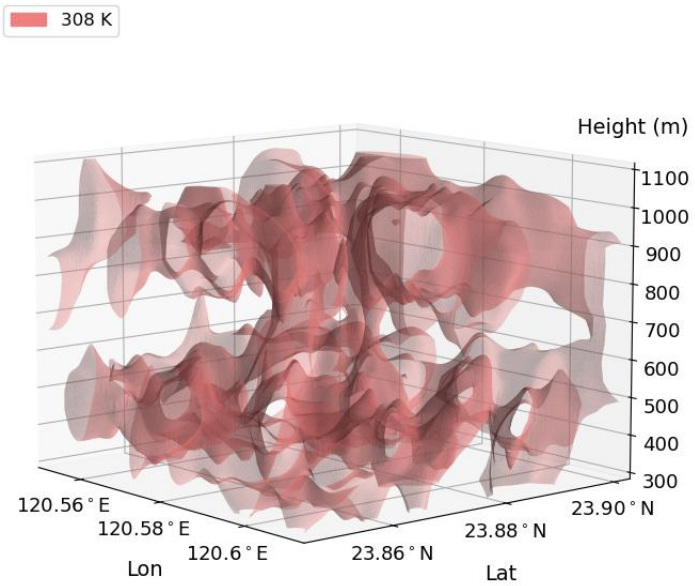

Figure 8 TPTRS-retrieved 3-D iso-surface of the potential temperature at 308 K at 1200 LST on 20 September 2023.

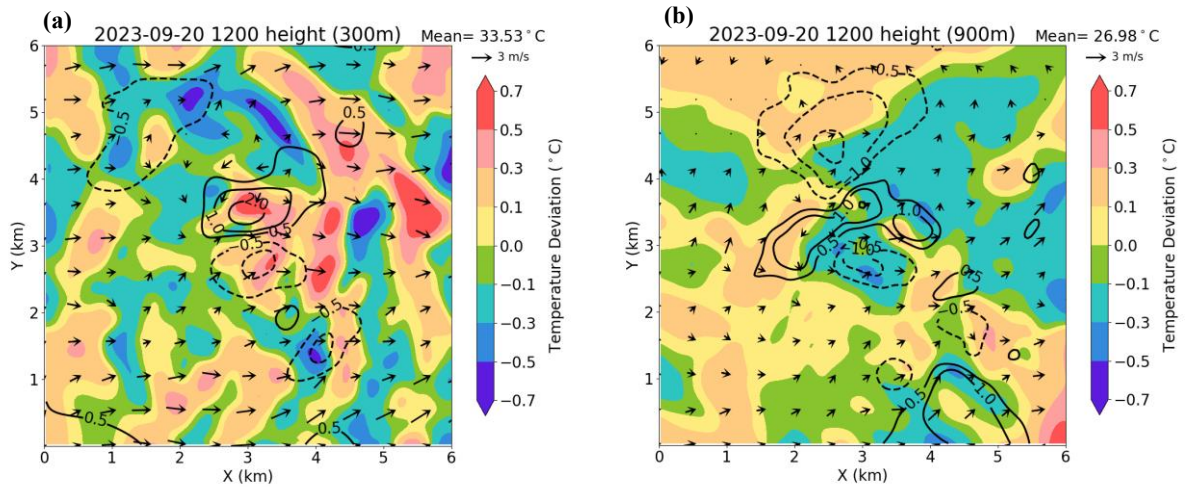

Figure 9 The retrieved temperature deviation from its horizontal average (in ^{o}C, color shading) at 1200 LST on 20 September 2023. The updrafts (solid line) and downdrafts (dashed line) with magnitudes at 0.5 m s^{-1}, 1.0 m s^{-1}, 2.0 m s^{-1}, and horizontal winds (arrows, plotted every 500 m) are superimposed. The heights are (a) 300 m; (b) 900 m.

3. Summary

This research demonstrates the advantages of using multiple Doppler scanning lidars and two advanced retrieval schemes to continuously provide 3-D wind and thermodynamic fields

within the boundary layer at a very high spatial resolution (50 m). Such synthesis methods and high-quality data sets could be applied for various purposes including the study of the boundary layer development, initiation of afternoon thunderstorms, air pollutant dispersion, numerical model verification, and real-time monitoring of aviation safety at airports.

4. References

[1] Liou, Y.-C., S.-F. Chang, and J. Sun, 2012: An application of the Immersed Boundary Method for recovering the three-dimensional wind fields over complex terrain using multiple-Doppler radar data. *Mon. Wea. Rev.*, **140**, 1603-1619, https://doi.org/10.1175/MWR-D-11-00151.1.

[2] Liou, Y.-C., P.-C. Yang, and W.-Y. Wang, 2019: Thermodynamic recovery of the pressure and temperature fields over complex terrain using wind fields derived by multiple-Doppler radar synthesis. *Mon. Wea. Rev.*, **147**, 3843-3857, https://doi.org/10.1175/MWR-D-19-0059.1.